Z-Gate Operation on a Superconducting Flux Qubit via its Readout SQUID

X. Y. Jin, S. Gustavsson, J. Bylander, F. Yan, F. Yoshihara, Y. Nakamura, T. P. Orlando, and W. D. Oliver

Phys. Rev. Applied **3**, 034004 — Published 11 March 2015

DOI: 10.1103/PhysRevApplied.3.034004

Z-gate operation on a superconducting flux qubit via its readout SQUID

X. Y. Jin,[1,*] S. Gustavsson,[1] J. Bylander,[1,†] F. Yan,[1] F. Yoshihara,[2,‡] Y. Nakamura,[2,3] T. P. Orlando,[1] and W. D. Oliver[1,4]

[1]*Research Laboratory of Electronics, Massachusetts Institute of Technology, 77 Massachusetts Avenue, Cambridge, Massachusetts 02139*
[2]*Center for Emergent Matter Science (CEMS), RIKEN, 2-1 Wako, Saitama 351- 0198, Japan*
[3]*Research Center for Advanced Science and Technology (RCAST), The University of Tokyo, 4-6-1 Komaba, Meguro-ku, Tokyo 153-8904, Japan*
[4]*MIT Lincoln Laboratory, 244 Wood Street, Lexington, Massachusetts 02420, USA*

(Dated: February 9, 2015)

Detuning a superconducting qubit from its rotating frame is one means to implement a Z-gate operation. In this work, we implement a Z-gate by pulsing a current through the qubit's readout dc SQUID. While the dc SQUID acts as a flux sensor for qubit readout, we in turn may use it as a flux actuator with tunable strength to impose a qubit frequency shift. Using this approach, we demonstrated Ramsey-type free-induction experiments with a time constants as long as 280 ns and rotation frequencies as high as 1.4 GHz. We experimentally demonstrated an inferred Z-gate fidelity of approximately 90%, limited largely by the bandwidth of our system. In the absence of this limitation, we argue that the inferred fidelity may be improved to as high as 99.0%.

I. INTRODUCTION

A quantum algorithm may be efficiently implemented on a quantum information processor using a universal set of one- and two-qubit gates [1]. The "Z-gate" is a single-qubit gate that often appears in such sets. This operation maintains qubit-state $|0\rangle$ and flips the sign of state $|1\rangle$, corresponding to a π rotation of the Bloch vector about the z-axis.

A Z-gate can be realized via a controlled frequency detuning of the qubit from its rotating frame. For superconducting qubits, one approach is to apply a rapid, adiabatic dc current pulse (voltage pulse) to a nearby antenna, which changes the qubit's magnetic flux bias (charge bias) and, thereby, its energy levels [2–5]. Such antenna-mediated biasing with adiabatic and non-adiabatic pulses has been used to facilitate single-qubit control and readout [6–10] and coupled-qubit interactions [11–18]. The coupling strength between the antenna and the qubit is generally static, fixed by their design, and this carries a fundamental trade-off for high-fidelity operations. Increasing the "always on" coupling strength will increase the gate speed, but also introduces more environmental noise. Conversely, reducing the coupling strength will reduce the environmental noise level, but at the cost of slower gate speed. An alternative approach is the use of multiple microwave gates to realize a Z-gate (i.e., via Euler rotations), but the need for multiple gates may also reduce the gate speed compared with a direct approach. A means to circumvent this trade-off is to introduce a tunable coupling which is strong only when needed.

Tunable couplers have been demonstrated in several superconducting qubit circuits for a variety of applications. For example, a current-biased Josephson junction was used in the quantronium qubit [19] both to enable qubit readout following noise-insensitive qubit operations and to implement a Z-gate [7]. In persistent-current qubits [20, 21], a dc SQUID was similarly used for qubit readout following degeneracy-point operation [22], as well as to increase coherence times by reducing environmental coupling due to junction asymmetry [23]. Furthermore, a dc SQUID [24] and a "coupler qubit" [25] have been used to mediate and tune the coupling between two persistent-current flux qubits. It is also worth noting that SQUIDs of this type have been used as resonators to read out qubits [26, 27], and its reduced geometry compared with a coplanar waveguide may be advantageous for scaling.

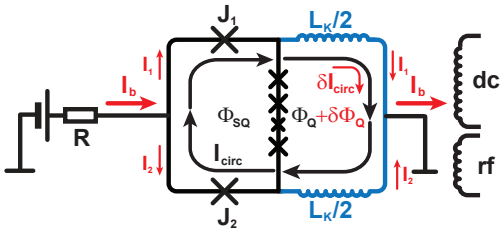

FIG. 1. Circuit schematic, comprising a SQUID (Josephson junctions J_1 and J_2) and persistent-current qubit (four series junctions "x"). A current in the "dc" inductor induces a magnetic-flux $\Phi_{\rm Q}$ in the qubit with persistent current $I_{\rm Q}$ (not shown), and $\Phi_{\rm SQ}$ in the readout SQUID with screening current $I_{\rm circ}$. The "rf" inductor is used to apply microwave flux pulses to drive qubit transitions. The SQUID and qubit loops share kinetic inductance L_K (blue), which, with a current $I_{\rm b} \equiv I_1 + I_2$, generates an additional circulating current $\delta I_{\rm circ} \equiv (I_1 - I_2)/2$ and an additional flux bias $\delta\Phi_{\rm Q} = L_{\rm K}\delta I_{\rm circ}$ to the qubit (see text for more detail). This shifts the qubit frequency an amount $\delta f_{\rm Q}$, implementing a Z-rotation.

In this paper, we implement a Z-gate operation on a persistent-current qubit using a dc SQUID, which serves as both a tunable coupler and a readout element (see Fig. 1). In the present context, the dc SQUID - qubit system has two key properties [28, 29]: 1) with no external current applied to the SQUID, the qubit is largely decoupled from the SQUID's

* jin@mit.edu
† Present address: Department of Microtechnology and Nanoscience, Chalmers University of Technology, SE-412 96 Gothenburg, Sweden
‡ Present address: National Institute of Information and Communication Technology (NICT), 4-2-1, Nukui-Kitamachi, Koganei, Tokyo 184-8795, Japan

external environment (coupling off condition), and 2) when an external current is applied to the SQUID, the qubit frequency is shifted, the qubit becomes coupled to the SQUID environment, and both increase with larger current amplitude (coupling on condition). By varying the SQUID current-pulse amplitude and duration, we can identify the combination of frequency shift, coupling strength, and pulse duration that realizes a Z-gate and maximizes its fidelity.

The frequency shift is also used to readout a persistent-current qubit operated at its high-coherence (degeneracy) point, where the two qubit states generate no net flux [22]. A current pulse is applied to the SQUID and passes through a kinetic inductance $L_{\rm K}$ which is shared with the qubit. This generates a magnetic flux offset that shifts the qubit to a higher-frequency bias point, where its states have net magnetization and are distinguishable by the dc SQUID magnetometer. When used for qubit readout, the SQUID is biased with a relatively large current-pulse amplitude, such that one of the two qubit states will cause the SQUID to switch to its normal state. In contrast, for a Z-gate, the current-pulse amplitudes will take only moderate values such that the SQUID always remains in the superconducting state.

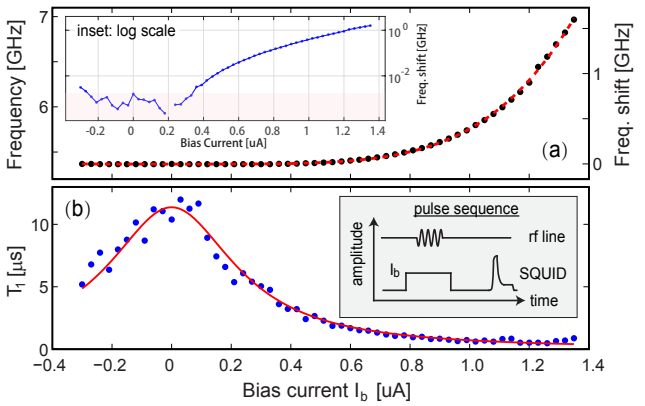

FIG. 2. Frequency shift $\delta f_{\rm Q}$ and energy relaxation time T_1 versus pulse amplitude I_b. (a) $\delta f_{\rm Q}$ versus I_b. The data (black dots) are fit (red line) using Eq. 3 to 4th order in $I_{\rm bs}$, with $\alpha = 1.0 \times 10^5$ A^{-1}, and $\beta = 1.6 \times 10^{16}$ A^{-3}. Inset: frequency shift on log scale. Data in pink region are not well resolved due to the frequency step-size used. (b) T_1 versus $I_{\rm b}$. Data (blue dots) are fit (red line) to $1/T_1 = 1/T_1^{(0)} + \kappa(I_{\rm b} - I_{\rm b}^*)^2$. $T_1^{(0)} = 12$ μs is the qubit's energy decay time at $I_{\rm bs} = 0$; $\kappa = 1.27\times10^{18}$ A^{-2}/s. Inset: pulse sequence of the experiment.

II. QUBIT MANIPULATION VIA SQUID LINE

The schematic of the sample is shown in Fig. 1. The qubit is a superconducting loop with geometric inductance $L_{\rm G}$ (not shown) interrupted by four junctions with a total Josephson inductance $L_{\rm Q}$. The qubit loop is galvanically connected with the SQUID via a shared kinetic inductance $L_{\rm K}$. The dc SQUID is designed to be symmetric, with two nominally identical Josephson junctions, J_1 and J_2, each having a critical current $I_{\rm c}$. A dc magnetic field B is applied to the qubit-SQUID system to position the qubit at its high-coherence bias point. Under most operating conditions, no external current is applied to the SQUID ($I_{\rm b} = 0$), and the circulating current $I_{\rm circ}$ is solely determined by the external field B.

The sample is designed such that $L_{\rm Q} \gg L_{\rm K} \gg L_{\rm G}$ (see supplementary material, Ref. 29), and this allows us to make the following conceptual simplifications:
(i) Since $L_{\rm Q} \gg L_{\rm K}$, an applied current $I_{\rm b}$ will mainly flow through the shared kinetic inductors $L_{\rm K}/2$, with negligible current dividing into the qubit junctions.
(ii) Since $L_{\rm K} \gg L_{\rm G}$, the contribution of $L_{\rm G}$ can be neglected.

During either qubit readout or Z-gate operation, a current $I_{\rm b} = I_1 + I_2 \neq 0$ is applied (I_1 and I_2 refer only to the extra currents associated with $I_{\rm b}$), and it splits down the two arms of the SQUID. In the presence of external field B, this splitting is not uniform, and it results in an *extra* circulating current $\delta I_{\rm circ}$. For a symmetric SQUID (*i*.e., identical junctions and inductances in each branch), $\delta I_{\rm circ}$ is an even function of $I_{\rm b}$ [30, 31]. In practice, small asymmetries may arise due to growth or fabrication variations, and these can be mitigated with a small offset current $I_{\rm b}^*$ [23, 28]. We define $I_{\rm bs} \equiv I_{\rm b} - I_{\rm b}^*$, in which $I_{\rm bs}$ is the bias current for a *symmetric* SQUID, $I_{\rm b}^*$ is a constant offset compensating the SQUID asymmetry, and $I_{\rm b}$ is the *applied* bias current. Then $\delta I_{\rm circ}$ can be expanded as an even function of $I_{\rm bs} \ll I_{\rm c}$,

$$\delta I_{\rm circ} = \alpha I_{\rm bs}^2 + \beta I_{\rm bs}^4 + \mathcal{O}(I_{\rm bs}^6). \tag{1}$$

The extra $\delta I_{\rm circ}$ leads to an additional flux bias on the qubit,

$$\delta\Phi_{\rm circ} = L_{\rm K}\delta I_{\rm circ}, \tag{2}$$

which, along with $\delta I_{\rm circ}$, is first-order insensitive to changes in $I_{\rm bs}$ near $I_{\rm bs} = 0$ [23, 28]. This is the coupler-off state.

Applying a current $I_{\rm bs}$ turns on the SQUID-qubit coupling and shifts the qubit frequency. Within a two-level approximation, the energy difference between the two lowest qubit eigenstates is $hf_Q = \sqrt{\Delta^2 + \varepsilon^2}$, in which h is Planck's constant, $f_{\rm Q}$ is the qubit frequency, ε is the energy difference between the qubit's classical circulating-current states, and Δ is their hybridization energy. In turn, $\varepsilon = 2I_{\rm Q}\delta\Phi_{\rm Q}$ is proportional to the qubit's circulating current $I_{\rm Q}$ and magnetic flux bias $\delta\Phi_{\rm Q}$, which is referenced to the qubit degeneracy point (*i.e.*, $\Phi_{\rm Q} = n\Phi_0/2$, $n = 0, \pm1, \pm2, \ldots$), where $\delta\Phi_{\rm Q} = 0$, $\varepsilon = 0$, and $hf_Q = \Delta$. Starting from this point, the extra flux $\delta\Phi_{\rm Q} = \delta\Phi_{\rm circ}$ induced when $I_{\rm bs} > 0$ increases the qubit frequency through the term $\varepsilon = 2I_{\rm Q}\delta\Phi_{\rm circ}$. Using Eqs (1) and (2), ε becomes

$$\varepsilon = 2I_{\rm Q}L_{\rm K}[\alpha I_{\rm bs}^2 + \beta I_{\rm bs}^4 + \mathcal{O}(I_{\rm bs}^6)], \tag{3}$$

and the resulting frequency shift $\delta f_{\rm Q}$ induced by the SQUID bias $I_{\rm bs}$ in the coupler-on state is

$$h\delta f_{\rm Q} \equiv h(f_{\rm Q} - f_{\rm Q}|_{\varepsilon=0}) = \sqrt{\varepsilon^2 + \Delta^2} - \Delta \tag{4}$$

To confirm these expressions, we performed spectroscopy measurements as a function of applied bias current $I_{\rm b}$. The flux qubit studied in this work has a qubit frequency $f_{\rm Q} =$

5.3662 GHz, energy relaxation time $T_1 = 12\,\mu$s and Hahn echo time $T_{2E} = 23\,\mu$s at the degeneracy point [29]. Experiments were performed in a dilution refrigerator operated at temperature $T = 20$ mK, such that $k_{\rm B}T \ll hf_{\rm Q}$, and the qubit is predominantly in its ground state in thermal equilibrium. At each $I_{\rm b}$ value, the qubit frequency $f_{\rm Q}$ is determined by fitting the resonance line with a Lorentzian. The qubit frequency $f_{\rm Q}$ (left axis) and corresponding shift $\delta f_{\rm Q}$ (right axis) are plotted versus $I_{\rm b}$ in Fig. 2a. The data fit well to $hf_Q = \sqrt{\Delta^2 + \varepsilon^2}$ (red dashed curve), in which ε in Eq. 3 is truncated at 4th order in $I_{\rm b}$, giving $\alpha = 1.0\times10^5$ A^{-1} and $\beta = 1.6\times10^{16}$ A^{-3}. Here $L_{\rm K} = 30$ pH and $I_Q = 0.18\ \mu$A are used [29].

We also measured the energy relaxation time T_1 as a function of $I_{\rm b}$ (Fig. 2b). T_1 changes minimally for small $I_{\rm b}$ values, where the qubit is first-order decoupled from the SQUID (see Eqs. 1 and 2). As $I_{\rm b}$ increases, the coupling to the SQUID and its environment becomes stronger and T_1 decreases. The T_1 value observed at the highest dc bias used in this work ($I_{\rm b} = 1.3\ \mu$A) is around 500 ns. The data are well fit to $1/T_1 = 1/T_1^{(0)} + \kappa(I_{\rm b} - I_{\rm b}^*)^2$, with $I_{\rm b}^* = 12$ nA, indicating that the reduction of T_1 is due to the SQUID environment. Note that $1/T_1 = \Gamma_1 = \frac{\pi}{2h^2}(\frac{\partial\varepsilon}{\partial I_{\rm bs}})^2 S_{I_{\rm bs}}$, in which $S_{I_{\rm bs}}$ is the current noise spectrum at the qubit frequency. From the fitting one is able to estimate the $S_{I_{\rm bs}} = 2h^2\kappa/64I_{\rm Q}^2L_{\rm K}^2\alpha^2\pi^2 = 6.06\times10^{-27}$ A^2/(rad s^{-1}), corresponding to zero-point fluctuations of a 200Ω impedance, and consistent with a similar device studied in Ref. [28].

III. Z-GATE (PHASE-GATE) OPERATIONS

To characterize the phase-gate operation, we performed Ramsey interferometry about the qubit quantization axis, the z-axis of the Bloch sphere (inset of Fig. 3e). The qubit starts in the ground state at its degeneracy point, $\varepsilon = 0$. A resonant $\pi/2$-pulse about the qubit x-axis was then applied via the microwave line (Fig. 1) to rotate the qubit Bloch vector to the y-axis. A Z-gate pulse was then applied via the dc-SQUID line, with an amplitude $I_{\rm bs}$ and duration $t_{\rm g}$. The gate pulse rise and fall times were rapid, but still adiabatic with respect to the qubit levels. This ensured that the pulse did not inadvertently drive transitions between the qubit states, even though the qubit's quantization axis is rotated during the pulse [29]. The qubit frequency increases during the pulse (see Eq. 4), and this induces free-precession of the qubit Bloch vector in the x-y plane about the z-axis at a rate equivalent to the frequency shift $\delta f_{\rm Q}$. After 1 μs, a second resonant $\pi/2$ pulse and a SQUID readout pulse were applied to measure the z-projection of the resulting qubit state (see Fig. 3). The phase-shift $\Delta\phi = 2\pi\int_0^{t_{\rm g}}(dt)\ \delta f_{\rm Q}$ accumulated in the x-y plane during the Z-gate operation is related to both the gate amplitude $I_{\rm bs}$, which sets the precession rate $\delta f_{\rm Q}$, and the gate duration $t_{\rm g}$, the free-precession time. Ideally, for a square pulse, this phase accumulation is given simply by $\Delta\phi = 2\pi\delta f_{\rm Q}(I_{\rm bs}) \times t_{\rm g}$. In practice, however, the phase accumulation rate may vary during the rising and falling edges of the gate pulse, necessitating a formal integration.

In Fig. 3a, we present one such a Ramsey experiment and plot the switching probability of the readout SQUID versus the effective gate amplitude $I_{\rm bs}$. When the gate amplitude is $I_{\rm bs} = 0$, the qubit is found in state $|1\rangle$ after the two consecutive $\pi/2$ pulses. As $I_{\rm bs}$ is increased, which in turn increases the frequency shift $\delta f_{\rm Q}$, the readout probability begins to oscillate between $|1\rangle$ and $|0\rangle$.

An arbitrary waveforem generator (AWG) was used to generate the pulse, comprising a triangle waveform with rise and fall times fixed at 1 ns. The 300-MHz bandwidth of the AWG led to a filtered realization of the ideal triangle waveform (inset Fig. 3a) The resulting pulse is well fit to a Gaussian pulse $V(t) = ke^{-t^2/2\sigma^2}$, in which $k = 0.76$ is the scaled amplitude, $\sigma = 0.34$ ns, and t is time. For a Gaussian current pulse with peak height of $kI_{\rm bs}$, the integrated phase accumulation is $\Delta\phi = 4\pi I_{\rm Q}^2L_{\rm K}^2/(h\Delta) \times \sigma\sqrt{\pi/2}\alpha^2k^4I_{\rm bs}^4$, in which ε in Eq. (3) is truncated at 2nd order in $I_{\rm bs}$. This phase accumulation is equivalent to that of a square wave with duration $t_{\rm g} = \sigma\sqrt{\pi/2}$ and amplitude $kI_{\rm bs}$. This allows us to convert the applied transient Gaussian pulse to an effective (constant current) gate amplitude of $kI_{\rm bs}$, and to fit the SQUID switching probability P_{SW} versus effective gate amplitude $I_{\rm bs}$ in Fig. 3a in a straightforward manner.

The solid red line in Fig. 3a is a fit to the data using the functional form $P_{\rm SW} = P_0 - A\cos(\Delta\phi + \phi_0)$, in which P_0 is the SQUID switching probability when the qubit is depolarized, A is the oscillation amplitude, and ϕ_0 is a phase offset of about 0.2 rad. The Gaussian pulse amplitude of $k = 0.79$ gives a best fit, and is consistent with the independently measured value 0.76 (inset Fig. 3a). The small difference is ascribed to the slight deviation of the pulse shape from an ideal Gaussian.

We next change both gate amplitude $I_{\rm bs}$ and gate width $t_{\rm g}$ to quantify the trade-off between gate speed (coupling strength) and coherence time (environmental noise). For each gate amplitude, we scanned the gate width to observe both the oscillation frequency and its decay time. We present the results for $I_{\rm bs} = 0.4\ \mu$A and $I_{\rm bs} = 1.0\ \mu$A in Figs. 3b and 3c, respectively.

In Fig. 3b, the lower $I_{\rm bs}$ corresponds to a weaker coupling; the qubit exhibits a relatively slower oscillation frequency (≈ 14.5 MHz) paired with a longer decay time (≈ 280 ns). As a result, only a few oscillations were completed before the system decayed. The small apparent variation in rotation frequency is ascribed to a low-frequency ringing of ≈ 10 MHz in the SQUID line. In Fig. 3c, the higher $I_{\rm bs}$ corresponds to a much stronger coupling; the qubit exhibits a faster rotation frequency (≈ 0.39 GHz) and a shorter decay time (≈ 48 ns). Despite the reduced coherence, many of the rapid oscillations can be completed within the shorter decay time.

It should be noted that the oscillation frequency is lower in the first 10 ns, and it increases to a steady-state value at larger $t_{\rm g}$. This is primarily due to bandwidth constraints within the measurement system (*e.g.*, pulse generator, external and on-chip filters), which increase the pulse rise-time and, therefore, the amount of time it takes the frequency shift to reach its steady-state value. The bandwidth limitation is exacerbated by the hyperbolic energy levels, which limits the frequency

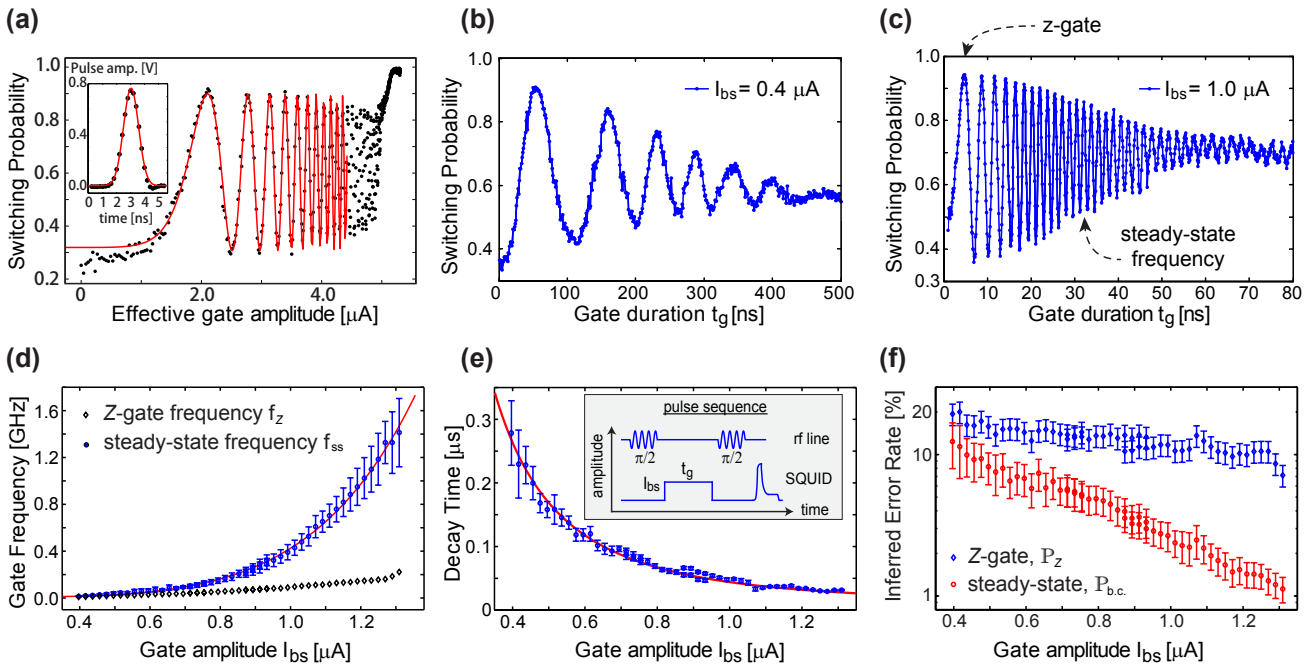

FIG. 3. Characterizing the Z-gate operation. (a) SQUID switching probability P_{SW} versus effective gate amplitude $I_{\rm bs}$ for a Gaussian pulse with fixed width. Data (black) are fit (red) with a cosinusoidal function with increasing frequency (see text). When $I_{\rm bs}$ approaches the critical current of the SQUID, the switching probability saturates to 100%. Inset: the applied triangle pulse with unity amplitude and 1 ns rise/fall times is filtered by the AWG to an approximate Gaussian with amplitude $k = 0.76$ (see text). (b) P_{SW} versus gate width $t_{\rm g}$, for $I_b = 0.4$ μA, (c) and for $I_b = 1.0$ μA. (d) Precession frequency of the demonstrated z-gate (f_Z, black) and in steady-state ($f_{\rm ss}$, blue) versus $I_{\rm bs}$. The steady-state data are fit (red line) using Eq. 1 to 4th order in $I_{\rm bs}$ (see text). (e) Ramsey decay time T_2^* versus $I_{\rm bs}$. The data (blue) are fit (red) using a quasi-static noise model (see text). Inset: Ramsey pulse sequence for the microwave and SQUID lines. (f) Experimentally demonstrated Z-gate error rate $\mathbb{P}_Z$ (blue circles) and inferred "best-case" error rate $\mathbb{P}_{\rm b.c.}$ (red circles) versus $I_{\rm bs}$ (see text).

shift for small pulse amplitudes. To quantify the actual and potential phase accrual rates, we define two quantities: the first is the actual Z-gate frequency $f_Z \equiv 1/(2T_Z)$, which corresponds to the experimentally demonstrated Z-gate duration T_Z in our system; and the second is the long-time steady-state frequency $f_{\rm ss}$, which corresponds to the "best-case" achievable rotation frequency for a given frequency shift. Using these definitions, we plot $f_{\rm ss}$ (closed circles) and f_Z (closed diamonds) versus I_b in Fig. 3d. Although the steady-state frequency can readily exceed 1 GHz, the experimentally demonstrated Z-gate frequency is at most 200 MHz, due primarily to the constraints described above.

In Fig. 3e, we plot the oscillation decay time (i.e., Ramsey T_2^* decay time) as a function of $I_{\rm bs}$. This is the relevant Z-gate decay time, and it decreases as the qubit's coupling strength to environmental noise is increased with increasing I_b. Since $T_2^* < 0.3\mu$s $\ll 2T_1 = 23\mu$s in this device, it follows that $T_2^* \approx T_\phi^*$, the inhomogenous pure dephasing time [32]. The observed decay function $\Gamma_2^* \approx \Gamma_\phi^* = 1/T_\phi^*$ is predominantly Gaussian, consistent with the dephasing being dominated by $1/f$ low-frequency noise. Furthermore, taking the low-frequency fluctuations to be Gaussian distributed and quasi-static (*i.e.,* constant during each free-induction period, changing to a new Gaussian-distributed value between periods) [33], the dephasing rate $\Gamma_\phi^* = 1/T_\phi^* \approx 1/T_2^*$ can be parameterized by an inhomogeneous flux (σ_Φ^2) and bias-current ($\sigma_{I_{\rm bs}}^2$) noise by

$$(\Gamma_\phi^*)^2 = 2\pi^2 \left(\frac{\partial f_{\rm Q}}{\partial \varepsilon}\right)^2 \left[\left(\frac{\partial \varepsilon}{\partial \Phi}\right)^2 \sigma_\Phi^2 + \left(\frac{\partial \varepsilon}{\partial I_{\rm bs}}\right)^2 \sigma_{I_{\rm bs}}^2\right] \quad (5)$$

in which the first term is the contribution of the flux noise, and the second term the contribution of the bias-current noise. Using the value for flux noise ($\sigma_\varepsilon^\Phi/h \equiv \frac{\partial \varepsilon}{\partial \Phi}\sigma_\Phi/h = 10$ MHz) measured independently on this device [29], the decay times in Fig. 3e correspond to a bias-current noise of $\sigma_\varepsilon^{I_{\rm bs}}/h \equiv \frac{\partial \varepsilon}{\partial I_{\rm bs}}\sigma_{I_{\rm bs}}/h = 3.7$ MHz $/\mu$A$\times I_{\rm bs}(\mu$A) This indicates that the bias-current noise can be comparable with the flux noise in limiting the Z-gate time.

Using the decay times (Fig. 3e) and the rotation frequencies (Fig. 3d), we can define an inferred experimental error rate for the demonstrated Z-gate,

$$\mathbb{P}_Z = 1/(2f_Z T_2^*), \quad (6)$$

which incorporates all experimental limitations through the use of the frequency f_Z; and a "best-case" inferred error rate which uses the steady-state frequency $f_{\rm ss}$,

$$\mathbb{P}_{\rm b.c.} = 1/(2f_{\rm ss} T_2^*). \quad (7)$$

The terms $2f_Z T_2^*$ and $2f_{\rm ss}T_2^*$ correspond to the number of π rotations that can be completed before the system decays for the experimentally demonstrated and "best-case" error rates respectively. Using these definitions, $\mathbb{P}_{\rm b.c.}$ and $\mathbb{P}_Z$ are plotted versus $I_{\rm bs}$ in Fig. 3f. Both error rates tend to decrease as I_b increases, indicating that the frequency ($\propto I_{\rm bs}^4$) increases faster than the decoherence rate $1/T_2^*$ ($\propto I_{\rm bs}^2$) as a function of $I_{\rm bs}$. At large $I_{\rm bs}$ values, for the experimentally achievable Z-gate, $\mathbb{P}_Z$ reduces to approximately 10%, corresponding to a demonstrated experimental fidelity $\mathbb{F}_Z \equiv 1 - \mathbb{P}_Z \approx 90\%$. For comparison, the "best-case" error rate, $\mathbb{P}_{\rm b.c.}$, would decrease to approximately 1%, corresponding to a "best-case" fidelity $\mathbb{F}_{\rm b.c.} \approx 99\%$. To improve the experimental fidelity, one obvious improvement is to increase the pulse bandwidth to approximately 1 GHz, using a higher-bandwidth AWG and filters with higher-frequency cut-off. Additionally, one can also improve gate fidelity by further increasing $I_{\rm bs}$. In this particular cooldown, however, the interaction of the qubit and a nearby two-level system [34] limited the range of $I_{\rm bs}$ to that shown in Fig. 3.

IV. SUMMARY

To conclude, we have demonstrated a Z-gate operation on a persistent-current qubit using the readout SQUID as a tunable coupler. In the present work, the SQUID served as both a readout element and the tunable coupler, although this is certainly not a requirement. The 90% inferred fidelity demonstrated here, while decent, is not yet competitive with state-of-the-art [35]. For example, we have demonstrated single-qubit gate fidelities around 99.8% via randomized benchmarking [36], and composite operations using these gates (*e.g.,* Euler rotations) would certainly yield a higher Z-gate fidelity. In this work, the experimentally inferred gate fidelity was primarily limited by the finite rise and fall times of our pulses, and addressing this issue will be the subject of future work.

ACKNOWLEDGEMENTS

We thank J. Miloshi, P. Murphy, R. Slattery, and T. Weir for technical assistance, and K. Harrabi for device fabrication. This research was funded in part by the Assistant Secretary of Defense for Research and Engineering under Air Force Contract No. FA8721-05-C-0002, by the U.S. Army Research Office (Contract No. W911NF-14-1-0078), and by the National Science Foundation (Grant No. PHY-1415514).

[1] M. A. Nielsen and I. L. Chuang, *Quantum Computation and Quantum Information* (Cambridge University Press, Cambridge, England, 2000).
[2] J. Clarke and F. K. Wilhelm, Nature **453**, 1031 (2008).
[3] J. Q. You and F. Nori, Nature **474**, 589 (2011).
[4] M. H. Devoret and R. J. Schoelkopf, Science **339**, 1169 (2013).
[5] W. D. Oliver and P. B. Welander, MRS Bulletin **38**, 816 (2013).
[6] Y. Nakamura, Y. A. Pashkin, and J. S. Tsai, Nature **398**, 786 (1999).
[7] E. Collin, G. Ithier, A. Aassime, P. Joyez, D. Vion, and D. Esteve, Phys. Rev. Lett. **93**, 157005 (2004).
[8] M. Steffen, M. Ansmann, R. McDermott, N. Katz, R. C. Bialczak, E. Lucero, M. Neeley, E. M. Weig, A. N. Cleland, and J. M. Martinis, Phys. Rev. Lett. **97**, 050502 (2006).
[9] K. Kakuyanagi, T. Meno, S. Saito, H. Nakano, K. Semba, H. Takayanagi, F. Deppe, and A. Shnirman, Phys. Rev. Lett. **98**, 047004 (2007).
[10] F. Deppe, M. Mariantoni, E. P. Menzel, S. Saito, K. Kakuyanagi, H. Tanaka, T. Meno, K. Semba, H. Takayanagi, and R. Gross, Phys. Rev. B **76**, 214503 (2007).
[11] Y. A. Pashkin, T. Yamamoto, O. Astafiev, Y. Nakamura, D. V. Averin, and J. S. Tsai, Nature **421**, 823 (2003).
[12] T. Yamamoto, Y. A. Pashkin, O. Astafiev, Y. Nakamura, and J.-S. Tsai, Nature **425**, 941 (2003).
[13] R. McDermott, R. W. Simmonds, M. Steffen, K. B. Cooper, K. Cicak, K. D. Osborn, S. Oh, D. P. Pappas, and J. M. Martinis, Science **307**, 1299 (2005).
[14] M. Steffen, M. Ansmann, R. C. Bialczak, N. Katz, E. Lucero, R. McDermott, M. Neeley, E. M. Weig, A. N. Cleland, and J. M. Martinis, Science **313**, 1423 (2006).
[15] T. Yamamoto, M. Neeley, E. Lucero, R. C. Bialczak, J. Kelly, M. Lenander, M. Mariantoni, A. D. O'Connell, D. Sank, H. Wang, M. Weides, J. Wenner, Y. Yin, A. N. Cleland, and J. M. Martinis, Phys. Rev. B **82**, 184515 (2010).
[16] M. Neeley, R. C. Bialczak, M. Lenander, E. Lucero, M. Mariantoni, A. OConnell, D. Sank, H. Wang, M. Weides, J. Wenner, *et al.*, Nature **467**, 570 (2010).
[17] L. DiCarlo, M. Reed, L. Sun, B. Johnson, J. Chow, J. Gambetta, L. Frunzio, S. Girvin, M. Devoret, and R. Schoelkopf, Nature **467**, 574 (2010).
[18] J. M. Martinis and M. R. Geller, Phys. Rev. A **90**, 022307 (2014).
[19] D. Vion, A. Aassime, A. Cottet, P. Joyez, H. Pothier, C. Urbina, D. Esteve, and M. H. Devoret, Science **296**, 886 (2002).
[20] J. E. Mooij, T. P. Orlando, L. Levitov, L. Tian, C. H. van der Wal, and S. Lloyd, Science **285**, 1036 (1999).
[21] T. P. Orlando, J. E. Mooij, L. Tian, C. H. van der Wal, L. S. Levitov, S. Lloyd, and J. J. Mazo, Phys. Rev. B **60**, 15398 (1999).
[22] I. Chiorescu, Y. Nakamura, C. J. P. M. Harmans, and J. E. Mooij, Science **299**, 1869 (2003).
[23] P. Bertet, I. Chiorescu, G. Burkard, K. Semba, C. J. P. M. Harmans, D. P. DiVincenzo, and J. E. Mooij, Phys. Rev. Lett. **95**, 257002 (2005).
[24] T. Hime, P. A. Reichardt, B. L. T. Plourde, T. L. Robertson, C.-E. Wu, A. V. Ustinov, and J. Clarke, Science **314**, 1427 (2006).
[25] A. O. Niskanen, K. Harrabi, F. Yoshihara, Y. Nakamura, S. Lloyd, and J. S. Tsai, Science **316**, 723 (2007).
[26] A. Lupaşcu, S. Saito, T. Picot, P. De Groot, C. Harmans, and J. Mooij, Nat. Phys. **3**, 119 (2007).
[27] J. C. Lee, W. D. Oliver, K. K. Berggren, and T. P. Orlando, Phys. Rev. B **75**, 144505 (2007).

[28] F. Yoshihara, K. Harrabi, A. O. Niskanen, Y. Nakamura, and J. S. Tsai, Phys. Rev. Lett. **97**, 167001 (2006).
[29] J. Bylander, S. Gustavsson, F. Yan, F. Yoshihara, K. Harrabi, G. Fitch, D. G. Cory, Y. Nakamura, J.-S. Tsai, and W. D. Oliver, Nat. Phys. **7**, 565 (2011).
[30] van der Wal, C. H., Wilhelm, F. K., Harmans, C. J.P.M., and Mooij, J. E., Eur. Phys. J. B **31**, 111 (2003).
[31] P. Bertet, I. Chiorescu, C. Harmans, and J. Mooij, arXiv preprint cond-mat/0507290 (2005).
[32] G. Ithier, E. Collin, P. Joyez, P. J. Meeson, D. Vion, D. Esteve, F. Chiarello, A. Shnirman, Y. Makhlin, J. Schriefl, and G. Schön, Phys. Rev. B **72**, 134519 (2005).
[33] F. Yan, J. Bylander, S. Gustavsson, F. Yoshihara, K. Harrabi, D. G. Cory, T. P. Orlando, Y. Nakamura, J.-S. Tsai, and W. D. Oliver, Phys. Rev. B **85**, 174521 (2012).
[34] S. Gustavsson, F. Yan, J. Bylander, F. Yoshihara, Y. Nakamura, T. P. Orlando, and W. D. Oliver, Phys. Rev. Lett. **109**, 010502 (2012).
[35] R. Barends, J. Kelly, A. Megrant, A. Veitia, D. Sank, E. Jeffrey, T. White, J. Mutus, A. Fowler, B. Campbell, *et al.*, Nature **508**, 500 (2014).
[36] S. Gustavsson, O. Zwier, J. Bylander, F. Yan, F. Yoshihara, Y. Nakamura, T. P. Orlando, and W. D. Oliver, Phys. Rev. Lett. **110**, 040502 (2013).